



RF Coil Setup for ^{31}P MRSI in Tongue Cancer *in vivo* at 7 T

Ria Forner^{1,2*}, Kyungmin Nam¹, Klijs J. de Koning³, Tijl van der Velden¹, Wybe van der Kemp¹, Alexander Raaijmakers^{1,4} and Dennis W. J. Klomp¹

¹ Division of Imaging and Oncology, University Medical Centre (UMC) Utrecht, Utrecht, Netherlands, ² Ceresensa Inc., London, ON, Canada, ³ Surgery, University Medical Centre (UMC) Utrecht, Utrecht, Netherlands, ⁴ Division of Biomedical Image Analyses, Technical University Eindhoven (TU/e), Eindhoven, Netherlands

OPEN ACCESS

Edited by:

Remy Guillevin,
Centre Hospitalier Universitaire (CHU)
de Poitiers, France

Reviewed by:

Simon Auguste Lambert,
Université Claude Bernard Lyon
1, France
Ivan V. Brak,
State Scientific Research Institute of
Physiology and Basic
Medicine, Russia
Roberta Frass-Kriegel,
Medical University of Vienna, Austria
Marek Chmellik,
University of Prešov, Slovakia

*Correspondence:

Ria Forner
RiaForner@gmail.com

Specialty section:

This article was submitted to
Applied Neuroimaging,
a section of the journal
Frontiers in Neurology

Received: 14 April 2021

Accepted: 10 September 2021

Published: 02 November 2021

Citation:

Forner R, Nam K, de Koning KJ, van der Velden T, van der Kemp W, Raaijmakers A and Klomp DWJ (2021) RF Coil Setup for ^{31}P MRSI in Tongue Cancer *in vivo* at 7 T. *Front. Neurol.* 12:695202. doi: 10.3389/fneur.2021.695202

Surgery for tongue cancer often results in a major loss in quality of life. While MRI may be used to minimise the volume of excised tissue, often the full tumour extent is missed. This tumour extent may be detected with metabolic imaging. One of the main reasons for the lack of metabolic information on tongue cancer would be the absence of an x-nuclear coil with the tongue as a focus target. Metabolic MRI through ^{31}P MRSI is known as a powerful tool to non-invasively study elevated cell proliferation and disturbed energy metabolism in tumours. Severe magnetic field non-uniformities are inherently caused by the substantial difference in magnetic susceptibilities of tissue and air in the mouth and its environs. Despite this, the wide chemical shift dispersion of ^{31}P could still facilitate precise detection of the cell proliferation biomarkers, phosphomonoesters and diesters, as well as energy metabolites ATP, inorganic phosphate, and phosphocreatine potentially mapped over the tongue or tumour *in vivo*. In this study, we present the first ^{31}P MRSI data of the human tongue *in vivo* from healthy volunteers and a patient with a tongue tumour at 7 T MRI using a ^1H 8-channel transceiver setup placed inside a body ^{31}P transmitter, which is able to get a uniform excitation from the tongue while providing comfortable access to the patient. In addition, a user-friendly external ^{31}P receiver array is used to provide high sensitivity (80%) comparable to an uncomfortable inner mouth loop coil positioned on the tongue. The primary aim is the demonstration of ^{31}P metabolite profiles in the tongue and the differences between healthy and malignant tissue. Indeed, clear elevated cell proliferation expressed as enhanced phosphomonoesters is observed in the tumour vs. the healthy part of the tongue. This can be performed within a total scan duration of 30 min, comparable to clinical scans, with a spatial resolution of 1.5 cm for the 10-min ^{31}P MRSI scan.

Keywords: ^{31}P MRSI, tumour, ^{31}P , RF coil, tongue, 7 T, UHF

INTRODUCTION

Amongst all intra-oral cancers, tongue cancer has the highest incidence, occurring in about 30% of all intra-oral cancer cases (1). The incidence rates vary globally, with high incidence rates in India and parts of Europe (1). While with surgery, the 5-year survival rates are on average 50–60% (2), the surgery itself has a significant impact on quality of life. A retrospective analysis in our centre showed that, in line with other literature (3), 84% of the resected specimens had inadequate resection margins (i.e., tumour cells <5 mm from the boundaries) (4). Inadequate resection margins are associated with low survival and are

therefore an indication to apply postoperative treatment in the oral cavity, i.e., re-resection and radiotherapy (5). Postoperative treatment has been reported in 35% of the oral cancer patients in our centre (15.5% re-resections and 19.5% radiotherapy), part of which could have been prevented by better margin control (6). Particularly, postoperative intraoral radiation may affect the quality of life of our patients due to significant morbidity and (oral) discomfort, including xerostomia, mucositis, fibrosis, and osteoradionecrosis.

To improve survival in patients with early tongue cancer, understanding the primary tumour extent is indispensable. In clinical practise, the extent of the primary oral cancer is evaluated by physical examination and imaging, e.g., MRI. Although MRI is regarded as the preferred imaging modality in OSCC (oral squamous cell carcinoma), it frequently underestimates as well as overestimates the extent of the tumour (7, 8). Inflammation surrounding the tumour could mimic or blur the boundaries that are observed in images (8). Therefore, improvements in MRI techniques are warranted to improve delineation of OSCC and subsequently decrease the rate of inadequate surgical margins (9). Conventional MRI makes use of extra-oral receive coils. Alternative MR imaging techniques, like MRI with an intra-oral coil, have been pioneered to assess tumour extent better. With an intra-oral coil, the highest sensitivity could be obtained for high-resolution anatomical MRI of the tongue (10). However, even in *ex vivo* MRI measurements where artefacts due to motion and field non-uniformity are minimal, surgical margins could not be assessed accurately in the anatomical MR images when compared to whole mount histopathology (11).

An alternative to imaging tumour extent based on anatomical characterisation is to investigate other image contrast mechanisms. Rather than observing water or its MR relaxation properties, one can also observe the energy and cell proliferation metabolism with MR, known to be substantially altered in tumour tissue. When observing ^{31}P MR spectroscopic imaging, one can reveal energy metabolites like PCr (phosphocreatine), ATP (adenosine tri-phosphate), Pi (inorganic phosphate), or cell proliferation markers like PMEs (phosphomonoesters) [PC (phosphocholine) and PE (phosphorylethanolamine)] and PDEs (phosphodiester) [GPE (glycerophosphorylethanolamine) and GPC (glycerophosphorylcholine)] (12, 13). Should the disturbed metabolic profile be visible post-surgery, it would indicate non-removal of tumour.

Relative proportions of metabolites indicate better response to different treatment plans. For instance, one may consider chemotherapy in cases where cell proliferation is high (i.e., high PME levels). However, the concentration of these metabolites is four orders of magnitude lower than water *in vivo*, while the gyromagnetic ratio of ^{31}P is also 2.5 times lower than that of ^1H . Consequently, for obtaining a comparable signal-to-noise ratio (SNR), the pixel size needs to be increased from sub-millimetre to more than a centimetre, i.e., increasing pixel volume by three to four orders of magnitude. Moving up in field strength from 3 to 7 T should further increase SNR more than two-fold (14).

It has been previously demonstrated that for ^{31}P MRSI (magnetic resonance spectroscopy imaging) in breast cancer even in Schmitz et al. (15), a small tumour of 6 mm in size, altered PME (PE+PC)/PDE (GPE+GPC) levels could be observed when

compared to healthy tissue despite partial volume effects and even in poorly B_0 shimmed areas (16). Due to the presence of sinus cavities, the B_0 homogeneity is less than ideal, which challenges the use of diffusion-weighted imaging (17). ^{31}P MRSI was considered possible as with this, there are no artefacts from highly abundant water or lipid signals, and the chemical shift dispersion of ^{31}P is so large that even in poor field uniformity, the peaks (PME and PDE) do not overlap. So, ^{31}P MRSI may be a good technical solution to the substantial B_0 shimming challenges exacerbated at 7 T, especially in the oral cavity due to the close proximity of air-filled cavities.

While dedicated receive-only tongue coils have been demonstrated for proton imaging *in vivo* at 3 T in combination with a body transmit coil, the required setup for ^{31}P is considered more complex. This complexity may be the reason for the absence of ^{31}P MRSI data of tongue tumours in literature. Local transmit-receive coils can be used for ^{31}P MRSI, but their non-uniform transmit field requires the use of adiabatic RF pulses. The resultant high levels of RF power deposition may violate SAR guidelines or compromise scan duration. Recently, it was shown that rather than a ^1H body coil, a ^{31}P body coil could be integrated into a 7-T MR system, using dipole antennas for ^1H transmit (18). This way, the ^{31}P setup could be substantially simplified, avoiding the need for adiabatic RF pulses and thus maintaining SAR guidelines within relatively short scan times. While other ^{31}P head coils (19, 20) have been reported in literature, these were optimised for brain imaging.

With the presence of such a built-in transmit coil for ^{31}P and an array of dipole antennas for ^1H imaging, the anatomy of the tongue would allow close proximal positioning of ^{31}P receive coils. An intra-oral coil placed supra-lingually would be ideally situated for maximum signal reception from the tongue. Unfortunately, there are two drawbacks to such a coil: (1) patients with painful tumours may not tolerate such a device for long periods, and (2) making the surface of the coil perpendicular to the static magnetic field and thus maximising signal requires holding the neck in an uncomfortable position for the duration of the scan protocols. So, keeping the subject's comfort in mind, an external coil would be more suitable.

In our study, we demonstrate the feasibility of ^{31}P MRSI of tongue cancer at 7 T. We present the design of a three-channel external ^{31}P Rx (receive) array, combined with a distal 8 channel TxRx (transceive) dipole array for ^1H excitation and reception placed inside a ^{31}P full-body Tx birdcage coil. In addition, we show that the SNR of the ^{31}P MRSI obtained in the tongue of healthy subjects when using the external array is comparable to the use of an intra-oral coil, highlighting the practically uncompromised added comfort of the external array. Finally, we demonstrate well-visible and distinguished signals from PME, PDE, PCr, Pi, and ATP with our setup mapped over the tongue in a patient with tongue cancer.

METHODS

Hardware

The ^{31}P and ^1H RF coil setup is composed of an embedded ^{31}P volume transmitter, an eight-channel ^1H TxRx dipole array mounted on a wide access cylinder, and a three-channel ^{31}P

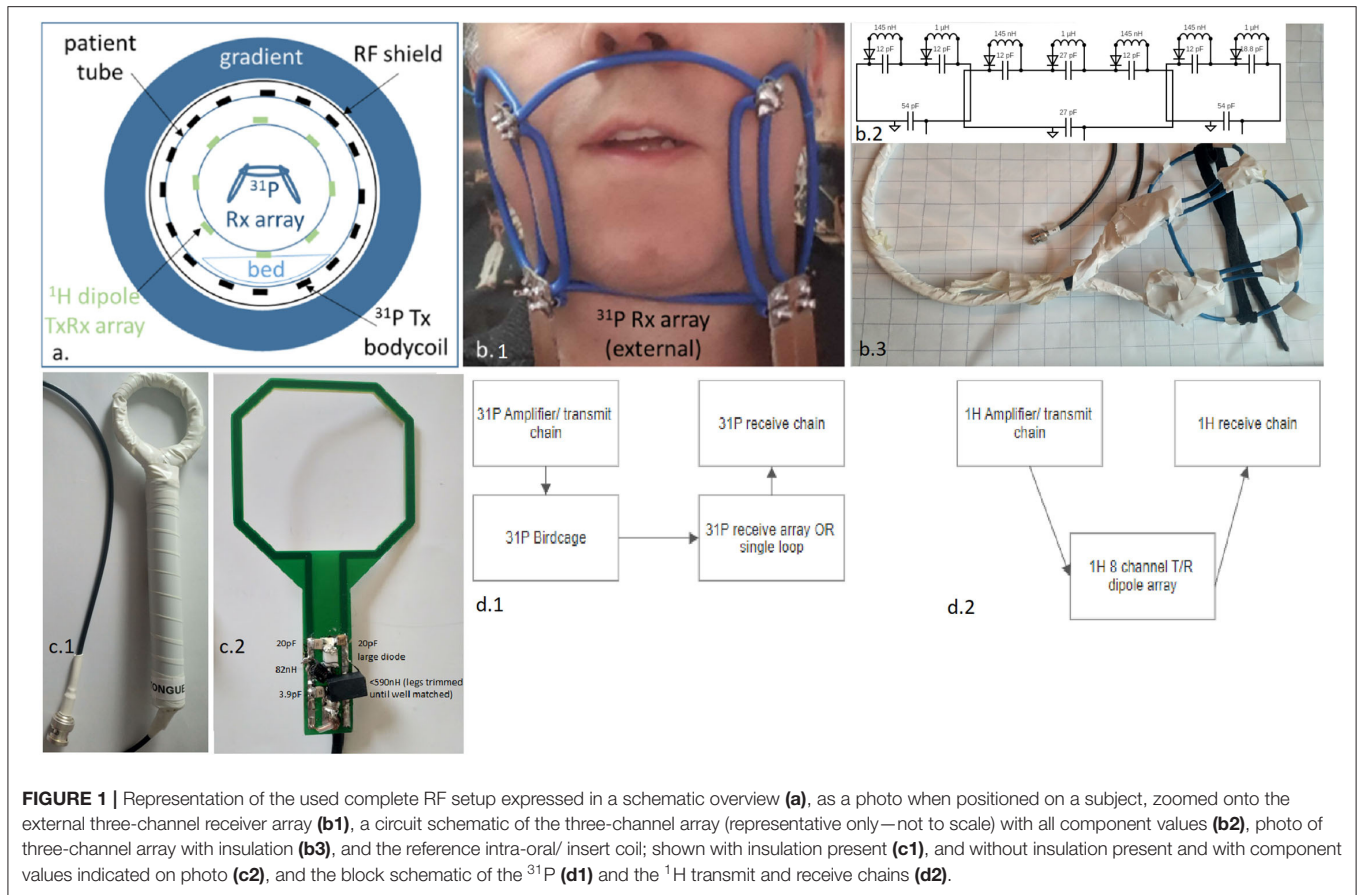


FIGURE 1 | Representation of the used complete RF setup expressed in a schematic overview (a), as a photo when positioned on a subject, zoomed onto the external three-channel receiver array (b1), a circuit schematic of the three-channel array (representative only—not to scale) with all component values (b2), photo of three-channel array with insulation (b3), and the reference intra-oral/ insert coil; shown with insulation present (c1), and without insulation present and with component values indicated on photo (c2), and the block schematic of the ³¹P (d1) and the ¹H transmit and receive chains (d2).

receiver array constructed as a face mask (see **Figures 1a,b** for visual representation). The ³¹P volume transmitter is a quadrature birdcage (21) driven with a two-channel (2×) 18-kW RF amplifiers (Analogic 8137, Boston Massachusetts). The ³¹P body birdcage (inside bore) is a pre-existing coil. All other coils mentioned, including the proton TxRx array, were purpose-built for this specific project.

¹H TxRx Dipole Array

The ¹H dipole array is based on the fractionated dipole design (22) and mounted on a 30-cm diameter Plexiglas former. The fractionated antennas have a length of 32 cm and have self-reflection parameters of −9 dB (worst case) when loaded with the human head. The dipole array was connected to the multi-transmit port of the 7 T MR system (Philips Healthcare, Best) that includes eight transmit/receive switches (duplexers) and can drive up to 2 kW per channel of RF peak power.

³¹P External Receive Array

The external three-channel ³¹P receiver array is composed of three partially overlapping loops, bent to approximate the curvatures of a typical face mask (see **Figure 1b**). The array is 24 cm across and has a width of 10 cm so as to adequately cover the field of view. The central, biggest loop has a diameter of about 12 cm, while the other two loops are about 9 cm each. Rigid 6-mm² isolated wire was used as conductors for the coil element.

Due to the rigidity of the loops, a mechanical frame was not needed. This allows for an open albeit electrically insulated (see **Figure 1** photo with and without insulation) frame such that the setup minimally impedes the respiration of the subject and reduces discomfort.

The central loop is positioned under the nose and reaches under the chin. This loop is opened in four locations, each connected to a small printed circuit board (PCB) with a tuning capacitor and detuning circuitry, as a consequence of the design and the four points of overlap with the neighbours. A minimum of two breaks were used to accommodate the segmenting capacitors for taking into account the wavelength and the total conductor length.

The remaining two loops are each opened in the two locations that match the crossing of conductors to provide the partial overlap and share the central loop’s PCBs. The two PCBs located to the chin’s left and right are equipped with matching capacitors and a wire-wound coaxial cable tuned with a capacitor to 120 MHz to ensure common mode current rejection (i.e., act as cable traps, not shown in electrical diagram, but embedded in PCB 1 and 2 shown in **Figure 1**).

Each Rx coil is tuned to the ³¹P Larmor frequency of 120 MHz and matched to 50 Ω when loaded with the face of an adult male and female. The ratios of unloaded to loaded Q factors for these loops are 4, when loaded with a human head. The three cables from the array are connected to an interface box that contains the

preamplifiers, a detuning malfunction check and interface to the MR system. The scanner checks the DC current to bias the PIN diode. Below a certain threshold, the scanner will abort or prevent scanning. Preamplifier decoupling was not implemented due to the inherent decoupling *via* overlap and strong tissue loading.

Comparison to Single Internal Loop

To compare the performance of the external array to a closely positioned internal coil, a single loop coil of 5 cm \times 6 cm was designed from a PCB, where the capacitors and detuning circuit are located just outside the mouth and the PCB is positioned directly on top of the tongue (**Figure 1c**). A 5-mm spacer enclosed in a latex housing was used to isolate the opened PCB from the tongue. Given the large wavelength at 120 MHz, differences in load sensitivity were not seen along the loop length. The coil was tuned to 120 MHz and matched to 50 Ω , and connected to the same interface as used for the external array. A ratio of 10 was seen for the unloaded and loaded Q factors.

RF Safety Assessment

^{31}P Body Birdcage

The design and dimensions of the ^{31}P body coil at 7 T are based on a classical 3 T body coil for ^1H in clinical MRI that operates on 128 MHz. Therefore, SAR settings from well-established 3 T MRI systems can be reapplied to the ^{31}P body coil, assuming all transmitted power to be absorbed by the subject, as described by Löring et al. (18).

^1H TxRx Dipole Array

The SAR of the ^1H dipole array was simulated in circularly polarised mode (Sim4Life, Zurich MedTech, Switzerland) using “Duke” as a model to determine the maximum average power based on peak local SAR and global SAR. As the ^1H setup is mostly used for brain imaging, the conventional quadrature drive would not be optimal when applied to the tongue. Since we intend to use the ^1H setup mainly for background imaging and B_0 shimming, we took a conservative approach where the per-channel power constraints were based on levels when driving the array with arbitrary phase settings and uniform power distribution over the eight elements (23). Considering that the head presents a different loading of the transmitter than the body for ^{31}P , and the performance of a coil (matching and tuning included) depends on loading, an *in vivo* flip-angle recalibration was performed with a human subject positioned with the tongue in the iso-centre of the magnet.

^{31}P External Receive Array

The ^{31}P local receiver coils are equipped with detuning circuits that prevent focusing of the RF power deposition in close proximity of the receiver coils. Bench tests (S_{12}) were performed to verify the performance of detuning by moving a small pickup probe over the conductor of the detuned receiver coil in the presence of an intrinsically uniform transmit field (using <1 dB as acceptance criteria). The procedure to test residual coupling is as follows: we start by detuning the Rx coil. Now, when the pickup probe (measuring the Tx field) is moved across the coil conductor (at the same distance as the closest load in the use case), half the

difference between the lowest and highest S_{21} values picked up by this coil quantifies the coupling. Less than 1 dB corresponds to <10% B_1 disturbance, which is in alignment with the scanner manufacturer specifications for receiver coils. The pickup loop is 1 cm in diameter.

As a secondary safety measure, a potential malfunction of the detuning circuitry was tested, in line with traditional ^1H commercially available receiver coils: The MRI system checks for the ability to drive a direct current (DC) within set boundaries through the detuning circuit and prevents scanning if the current exceeds specifications. The malfunction detection circuit was tested by deliberately opening the DC circuit during a scan and verifying that the scan immediately aborts.

In terms of the loading, proximity and hence the SAR *in vivo*, the internal loop coil has the highest risk of violating SAR requirements. As a result, the external coil was not as rigorously tested due to the inherently insignificant risks.

^{31}P Internal Receive Loop

Finally, for the insert coil, a B_1^+ map at the ^1H frequency was obtained, once with and once without the presence of the receiver coil to verify the absence of local B_1^+ alterations caused by the receiver (24).

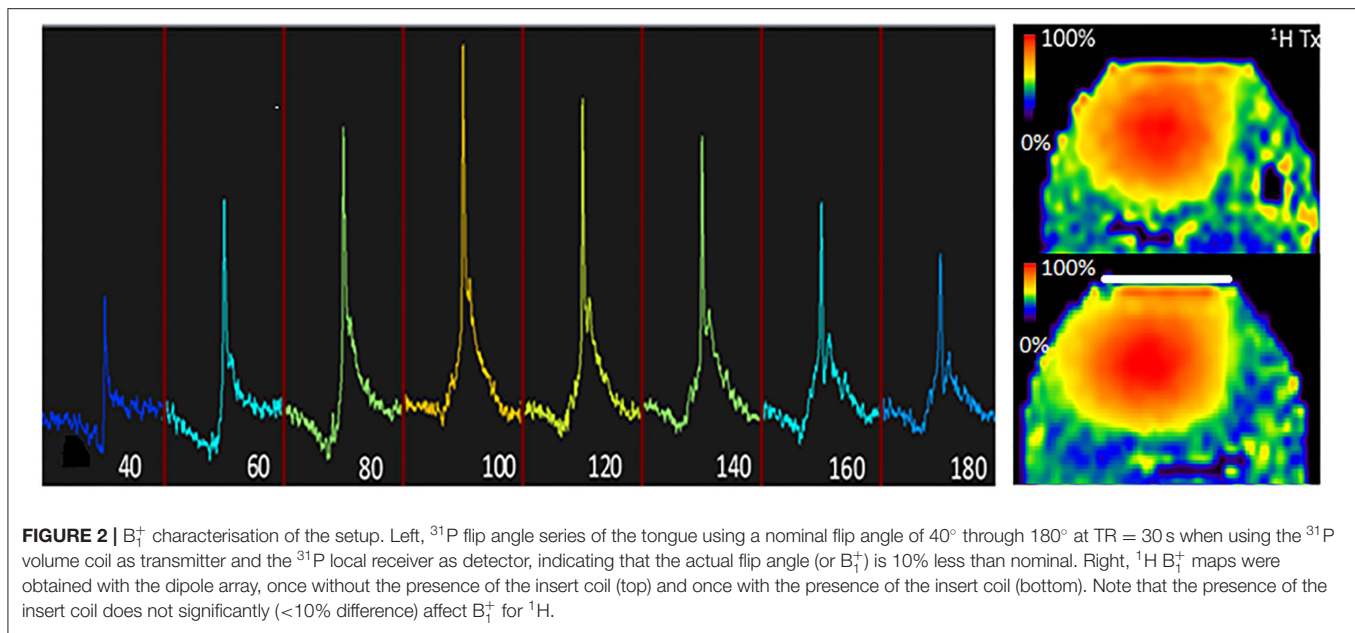
Subjects

A total of three volunteers were enrolled in this study. All gave written informed consent and the protocol development was approved by the local ethical committee. Moreover, the non-commercial ^{31}P and ^1H transmit setup was described in an investigation medical device dossier, which was approved by an independent auditing board. Subject 1 (female, 30 years) was scanned once with the internal coil (**Figure 1c**) and once with the external array (**Figure 1b**). Subject 2 (male, 46 years) was scanned with the external setup. Finally, subject 3, a patient with tongue cancer (male, 68 years), was scanned with the external setup. Subjects were instructed to avoid movement for the ^1H scans as well as the 3D CSI. They were recommended to touch the tip of their tongue to the front teeth, although considering the presence of painful tumours, this may not have been practicable for all.

Scan Protocol

The assessment of potential coupling of the ^1H antennas to the ^{31}P insert coil was verified by phantom measurement in a 10-cm Perspex sphere filled with physiologic salt (0.9% NaCl). This sphere contains two additional smaller solution-filled spheres, the first containing 200 mM of Pi and the other containing 50 mM each of PC, PE, and GPC. The reader's attention is drawn to the fact that this was done merely to check the starting values for the *in vivo* setup and that a flip angle series was further performed *in vivo* for quantification. A 3D B_1^+ map (25) was obtained for ^1H with a spatial resolution of 2 \times 2 \times 10 mm, with and without the presence of the insert coil for comparing the difference in the B_1^+ map as shown in **Figure 2**.

In one subject, the ^{31}P flip angle series was obtained using a rectangular RF pulse with a repetition time of 10 s and increasing B_1 amplitude up to the maximum available power



of the RF amplifier. The carrier frequency was set to the PCr resonance, and the nominal flip angle ranged from 40° until 180° with a 20° interval, using the volume transmitter. The local ^{31}P insert receiver was used to localise the signal to the tongue.

A multi-slice image in the rapid gradient echo sequence (FFE) was acquired to determine the tongue's location within the head of the subject. The field of view was set to $224 \times 224 \times 82.5$ mm and a voxel size of $2.33 \times 2.33 \times 5.5$ mm. The flip angle was set to 10° , with a TE of 1.25 ms, TR of 30 ms, and a single average with a slice thickness of 5 mm. For the first-order B_0 shimming, a 3D B_0 map was obtained ($\Delta\text{TE} = 1$ ms). The FWHM (full width of the peak at half the maximum amplitude) linewidth of the distribution of B_0 offset in the tongue area is reported, after which the carrier frequency is fixed to water for ^1H and by fixed ratio automatically to PCr for ^{31}P .

The 3D ^{31}P MRSI data were acquired in a field of view of $224 \times 224 \times 150$ mm with a spatial resolution of $15 \times 15 \times 15$ mm isotropic with a 5-kHz bandwidth. The acquisition window was set to 50 ms (i.e., spectral 20 Hz resolution) to allow a short TR of 57 ms, TE of 0.61 ms, and an optimal flip angle of 10° . The maximum B_1^+ was $6 \mu\text{T}$. Hamming weighted acquisition was applied with 50 averages of the centre parts of k-space resulting in a total scan time of 10 min for the ^{31}P MRSI scan. Afterwards, the reconstruction was performed following noise de-correlation, averages, spatial Hamming filtering, channel combination [whitened singular value decomposition (WSVD) (26)], 20 Hz spectral line broadening, fixed first-order phase correction, and automated zero-order phase correction using the CSigui toolbox (27). The total scan session, including the proton scans, adds up to a total scan duration of at least 30 min, sometimes stretching up to 60 min in case of repeated scans due to subject motion.

RESULTS

^{31}P Receive Performance on the Bench

Bench-top S_{12} measurements confirmed that in the detuned state, the receivers caused <1 dB of B_1 field disturbance in close proximity of the conductors. When comparing the S_{12} between a perfectly aligned small pickup probe positioned on top of the centre of the tongue to each of the loops of the external array, about 6 dB (centre coil) or 7 dB (left and right coil) of loss was observed when compared to the internal coil.

External Array

All subjects could comfortably be positioned in the setup when using the external array. The insert loop was considered very uncomfortable as it causes substantial accumulation of saliva, and swallowing is complicated and influences coil placement. Moreover, the head needs to be bent forward to ensure an orthogonal orientation of the loop with respect to the main field of the magnet to ensure highest SNR, which was experienced as uncomfortable. Nonetheless, one subject could successfully complete the ^{31}P MRSI study with the insert coil as the receiver in place.

When comparing the ^{31}P results from the three healthy subjects, it can be observed that the SNR is substantially variable; however, in all voxels from the tongue, resonances of PCr, ATP, PME, and/or PDE and Pi could be observed (Figure 3).

All three elements of the external array contributed to the signal for the ^{31}P MRSI of the patient, albeit one element showed overall lower signal intensity (Figures 4a–c). Using WSVD to combine the signals, ^{31}P MRSI was successfully obtained and processed, showing spectra distributed all over the tongue (Figure 4d).

When taking a closer look at the spectrum from the tumour area, one can see a substantially elevated signal of PME when

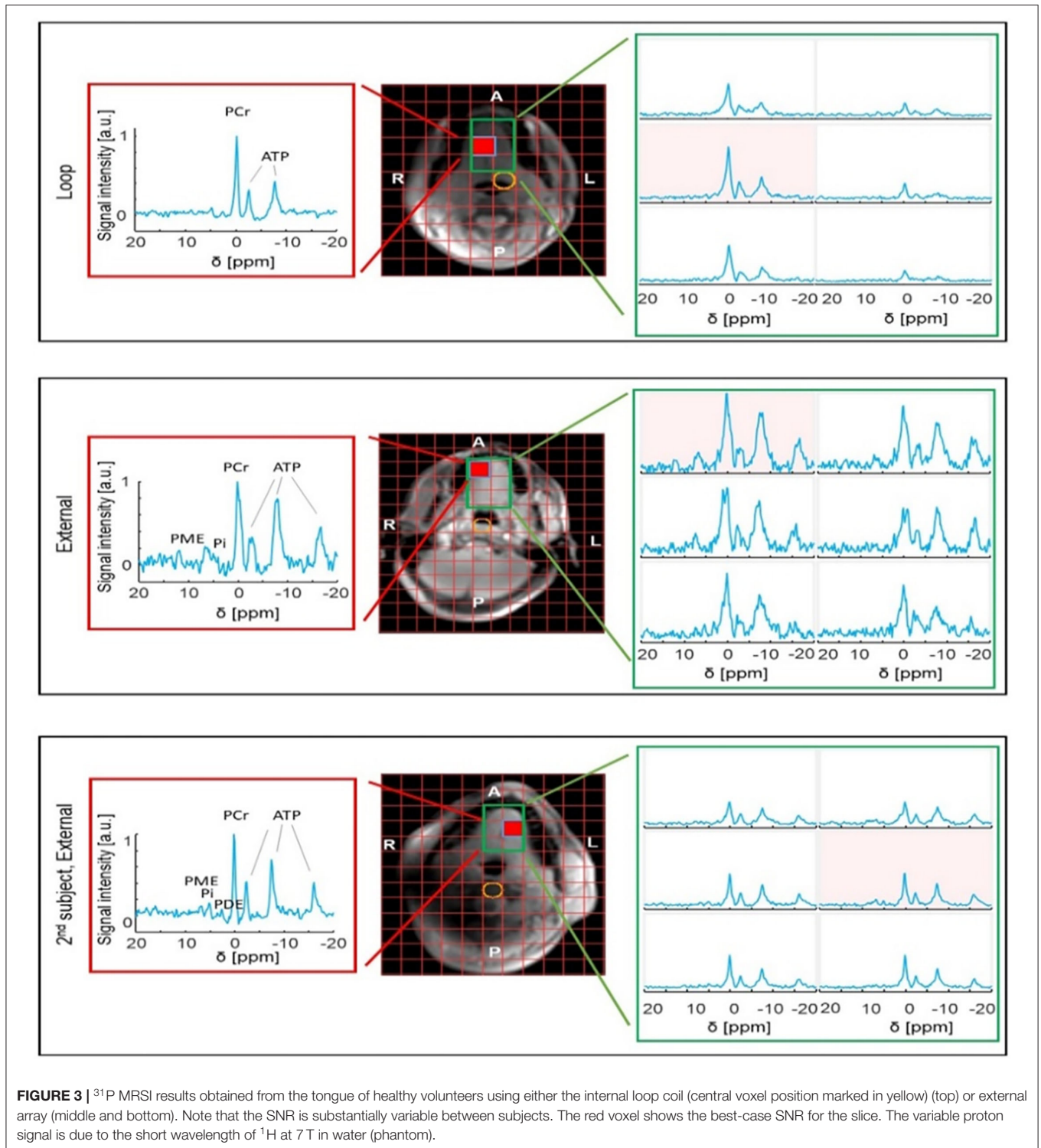
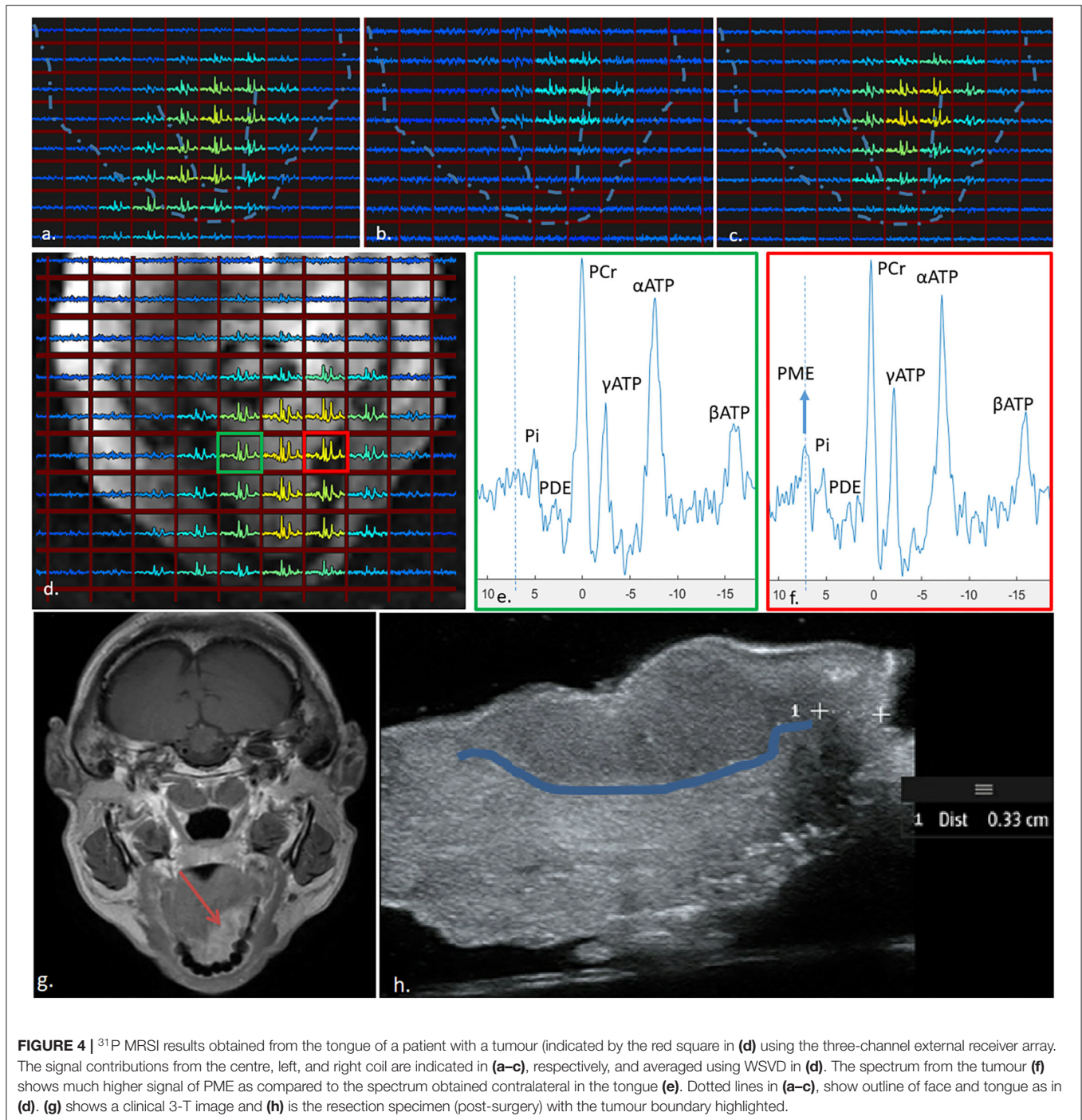


FIGURE 3 | ³¹P MRSI results obtained from the tongue of healthy volunteers using either the internal loop coil (central voxel position marked in yellow) (top) or external array (middle and bottom). Note that the SNR is substantially variable between subjects. The red voxel shows the best-case SNR for the slice. The variable proton signal is due to the short wavelength of ¹H at 7 T in water (phantom).

compared to a spectrum from a contralateral (healthy) region of the tongue (Figures 4e,f). For reference, a clinical 3T MRI image is shown in Figure 4g, and the excised tongue post-surgery is shown in Figure 4h with the tumour boundary demarcated.

Comparison to Internal Loop

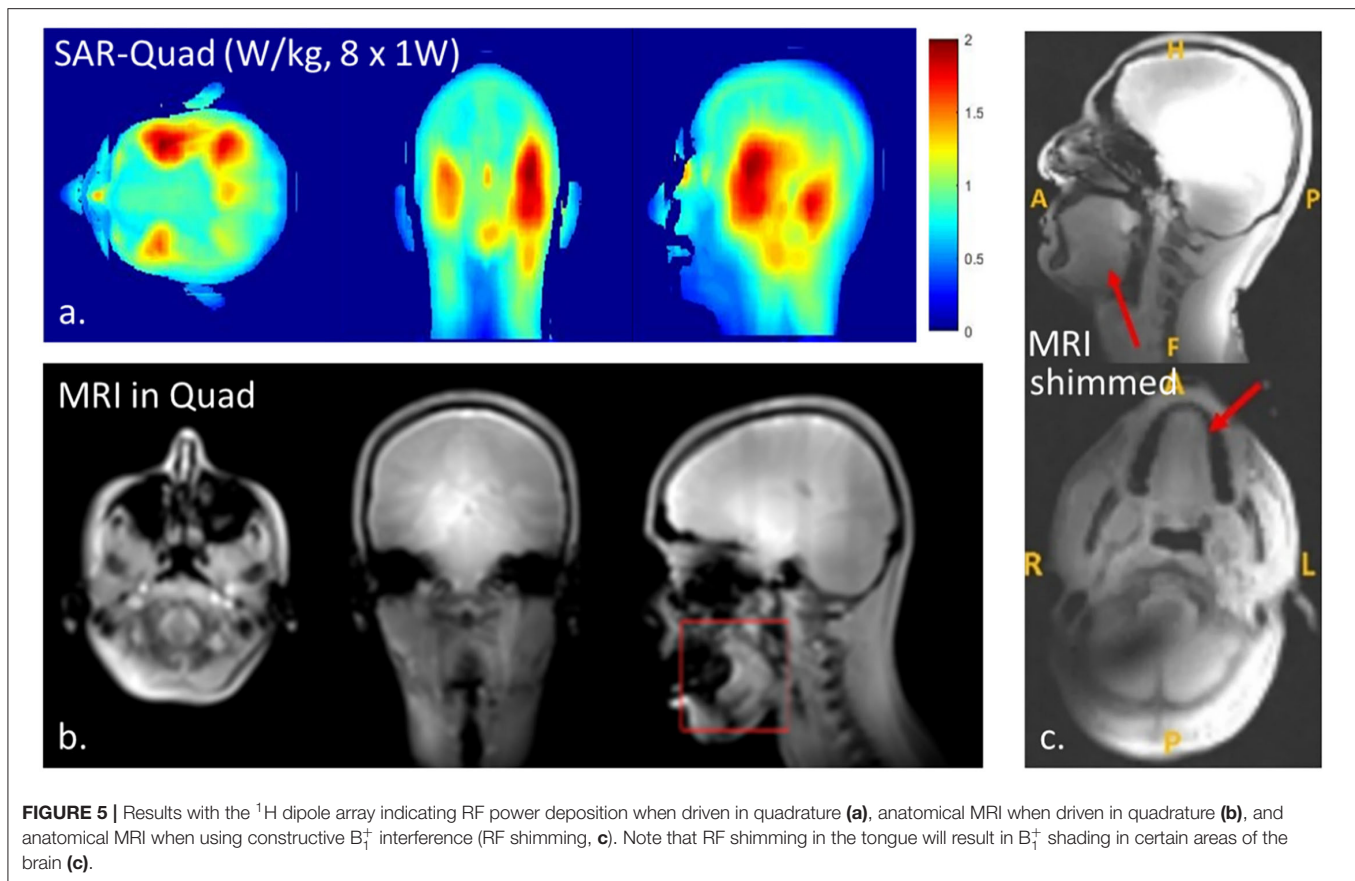
When comparing the maximum SNR of the external array with the loop coil on the same subject, about two to three-fold reduced SNR is observed in the array. However, note the substantially



increased SNR towards one side of the tongue, close to the jaw muscle. When comparing the SNR of the second subject to the first subject both obtained with the external array, in the second subject, about two-fold more SNR is observed. Overall, the signal levels over the tongue are substantially more uniform with the external array when compared to the loop coil. The array acquires signal from the entire mouth cavity as opposed to the internal coil, which is sensitive only to a portion of the tongue.

^{31}P Transmit Performance

A flip-angle series using the ^{31}P body coil as transmitter and the insert ^{31}P coil as receiver indicated a maximum signal when the nominal flip angle was 100° (**Figure 2**, left) at a TR of 30 s. While shielding between the Tx birdcage and the ^{31}P tongue coils might be expected due to the presence of the ^1H dipoles, this is not seen in practise. The dipoles resonate far off the ^{31}P frequency and there is sufficient distance between these two coils (18).



^1H TxRx Dipole Array

The presence of the ^{31}P insert coil did not alter the ^1H B_1^+ field of the dipole array significantly (i.e., differences of $<10\%$) in a phantom as shown by the comparison between the B_1^+ maps with or without the presence of the ^{31}P insert coil (Figure 2, right).

RF simulations of the eight-channel dipole array resulted in a peak SAR of 1.94 W/kg and a global SAR of 0.6 W/kg when driven in quadrature at 1W delivered power for each channel (Figure 5a). When driven at 1W with an arbitrary phase between the elements, the worst-case local SAR (23) could increase to a maximum of 7.3 W/kg. For all subjects, we have used RF shimming by means of constructive B_1^+ interference in the tongue. To ensure that we remain within the 10 W/kg peak local SAR in the head (28), we set the maximum allowable power per channel to 1.37 W ($1\text{W} \times 10\text{W/kg} / 7.3\text{W/kg}$).

Figure 5 demonstrates anatomical MR images obtained from one of the volunteers using the dipole array driven in quadrature (Figure 5b) and with RF shimming on the tongue (Figure 5c). The anatomical MR images were sufficient for region-of-interest B_0 shimming. Determining the optimal phase combination for constructive B_1 shimming took <10 min and was successful in all subjects. While up to third-order B_0 shimming is available, the B_0 field uniformity in the tongue could not be better than 40 Hz, expressed as FWHM (full-width at the half of the maximum of the peak) of the offset frequencies of

water. Since shimming varies per subject, positioning, tissue coupling, etc. shim values accordingly differ, yet since the shim procedure is automated, we have not noted the actual phase settings.

DISCUSSION

By combining proton antennas with a traditional full-body birdcage for ^{31}P transmit and a dedicated receive array, we present, what is to our knowledge, the first RF coil setup at 7 T for ^{31}P MR spectroscopy in the buccal region and tongue. First, we confirmed negligible coupling between the proton array and the phosphorus receive coils to demonstrate safety. The coupling between the two transmit coils has been previously noted to have been insignificant (18). In our study, we have used the SAR setting that allows arbitrary phase setting between channels (which is three-fold more conservative than for quadrature drive).

Next, we have compared the ^{31}P performance of a comfortable external receiver array to a close-fitting uncomfortable insert coil. Finally, we have detected a first indication of altered cell proliferation by means of elevated PME levels in the tumour vs. the contralateral healthy area of the tongue in a patient.

Dedicated receiver arrays for MRI of tongue cancer have been presented for proton imaging. Voskuilen et al. (29) could indeed demonstrate a factor of two gain in sensitivity at 3 T in

the tongue when comparing their 12-channel array positioned close to the mouth to a commercially built head-neck coil. In addition, inserted ¹H coils have been proposed at 4 T to perform MRI while the coil is inside the mouth, again showing excellent sensitivity (10). However, they also acknowledged the sub-optimal alignment of the insert coil with respect to the main magnetic field. In our *in vivo* bench test observations that are independent of field orientation, we observed about 6–7 dB loss in B₁ for each element of the array when compared to a closely positioned insert coil. With optimal signal combination and assuming negligible coupling between elements, based on these bench-top measurements, the sensitivity of the external array is about 80% of the sensitivity of the internal coil, i.e., $\frac{10\sqrt{\frac{7}{20}} + 10\sqrt{\frac{6}{20}} + 10\sqrt{\frac{7}{20}}}{\sqrt{3}}$. While the sensitivity comparison between coils is difficult to assess in a practical ³¹P MRSI experiment, it can be recognised that the insert coil could provide more SNR, albeit the external array provides a more uniform signal detection over the entire tongue area. While the tip of the tongue is indeed thin, the start of the tongue is relatively thick (see also anatomic MRI). For the tip of the tongue or when tumours are close to the surface, a thin insert coil should provide better SNR. However, in practise, due to the uncomfortable setup, the success rate of a clinical study may be worse. The receive array does not have preamplifier decoupling implemented. Further gains in performance could be obtained by trimming the cable length to optimise it for preamplifier decoupling.

In our study, we used an embedded bore coil as a ³¹P volume transmitter. Previous studies (18, 27, 30) have shown the benefits of a relatively uniform transmit field for ³¹P excitation. It extends the field of view, simplifies RF power calibration, and facilitates the use of Ernst-angle optimised scans for the highest SNR. Making the best out of the compromised magnetic field uniformity in the mouth at 7 T, we could use a relatively short acquisition window that matches the corresponding relatively short T2* to allow a short TR of 57 ms, thus high SNR per unit of time. Moreover, the short TR facilitates the acquisition of many k-points to spatially encode the signal in 3D while being capable of substantial signal averaging of the centre of k-space to match the optimal Hamming weighted acquisition (31).

The magnetic field uniformity was at best 0.13 ppm (40 Hz/298 MHz). Moreover, swallowing and subtle movements during the 10-min MRSI scan can cause more line broadening of the spectra (32). Owing to the large chemical shift dispersion of ³¹P, even in the presence of motion and non-uniform magnetic fields, resonances of PME, Pi, PDE, PCr, and ATP could be well-resolved, which is a distinct advantage over ¹H spectroscopy. Further improvements in magnetic field shimming and motion correction strategies could be considered when aiming for resolving phosphoethanolamine and phosphocholine peaks of the PME signal (33). For instance, using local shim coils or advanced shimming strategies may improve magnetic field uniformity (34). Even prospective motion correction may be considered to improve the linewidth of the spectra (35).

Recently, other dedicated ³¹P coil setups have been demonstrated for 7 T for brain imaging (19, 20). These state-of-the-art head coils have indicated more than a factor 3 in SNR

performance gain when comparing their array with the typical volume coil. While we optimised our MRI setup to acquire the ³¹P MRSI specifically in the tongue, we did incorporate an eight-channel transmit/receive dipole array for proton MRI. Although not fully exploited in this study, phase and amplitude B₁⁺ shimming could significantly improve MRI quality (36). Consequently, the setup may be used for imaging multiple contrast mechanisms in addition to phospholipids and energy metabolism. Recently, Kappert et al. have shown that diffusion-weighted MRI can be used successfully in the tongue (17). Moreover, Athar et al. (37) confirmed that MRI using contrast enhancements could provide 83% accuracy in determining the tumour thickness when compared to histopathology, advising to use MRI for treatment planning in patients with tongue cancer. Potentially, multiple relevant tumour biomarkers like elevated cell proliferation, altered energy metabolism, disrupted perfusion, and hindered diffusion may be studied in patients with tongue cancer to improve treatment decisions.

Our proposed setup was demonstrated to be suitable for metabolic tongue imaging. The proton multi-transceiver system allows for B₁ shimming to provide proton MRI and B₀ shimming, the latter being crucial considering the large air pockets of the sinus cavities. However, even though one subject had solid gold fillings, no adverse B₀ homogeneity artefacts were detected. Similarly, relatively uniform ³¹P excitation could be obtained without the hindrance of the coil since the setup was hidden behind the bore liner of the MRI. Since the ³¹P receive array could be positioned like a face mask, comfortable 3D MRSI could be obtained from the tongue. While the 3D CSI scan itself takes only 10 min, with additional time due to tailor the preparation scans, the scan session, including the proton scans, adds up to a total scan duration similar to clinical MRI scan sessions.

Spatial resolution of the ³¹P MRSI scan is still compromised to 1.5 cm for the 10-min scan. While higher resolutions can be obtained, it will come at the expense of longer scan times or less SNR. However, it should be noted that despite lower spatial resolution, the effect size in metabolite level can be substantial, so even with partial volume effects, alterations may still indicate tumour extent.

CONCLUSION

Here, we have demonstrated a novel coil setup and scan protocols for phosphorus spectroscopy as a means for detecting altered cell proliferation and energy metabolism in tongue tumours. To begin with, we compared the performance of the patient-friendly external three-channel receive array to the ideal case of an intra-oral loop and noticed 80% sensitivity performance of the external array with respect to the inner coil. As an improvement over commercially available head coils, we have used a surface loop array that is inherently decoupled from the proton coil and provides full coverage of the tongue. This setup builds the first steps towards aiding surgery treatment decisions using patient spectroscopy data, even in traditionally hard-to-image anatomic regions such as the mouth.

DATA AVAILABILITY STATEMENT

The raw data supporting the conclusions of this article will be made available by the authors, without undue reservation.

ETHICS STATEMENT

The studies involving human participants were reviewed and approved by Medisch Ethische Toetsingscommissie (METC) Utrecht; UMC Utrecht. The patients/participants provided their written informed consent to participate in this study.

AUTHOR CONTRIBUTIONS

RF: hardware, safety tests, scans for data acquisition, written drafts, and figures. KN: scans for data acquisition, sequence modification, writing, and figures. KK: patient scans and writing.

REFERENCES

- Moore S, Johnson N, Pierce A, Wilson D. The epidemiology of tongue cancer: a review of global incidence. *Oral Dis.* (2008) 6:75–84. doi: 10.1111/j.1601-0825.2000.tb00105.x
- Marra A, Violati M, Broggio F, Codecà C, Blasi M, Luciani A, et al. Long-term disease-free survival in surgically-resected oral tongue cancer: a 10-year retrospective study. *Acta Otorhinolaryngol Ital.* (2019) 39:84–91. doi: 10.14639/0392-100X-2336
- Smits RWH, Koljenović S, Hardillo JA, ten Hove I, Meeuwis CA, Sewnaik A, et al. Resection margins in oral cancer surgery: Room for improvement. *Head Neck.* (2016) 38:E2197–E203. doi: 10.1002/hed.24075
- de Koning KJ, Koppes SA, de Bree R, Dankbaar JW, Willems SM, van Es RJJ, et al. Feasibility study of ultrasound-guided resection of tongue cancer with immediate specimen examination to improve margin control - Comparison with conventional treatment. *Oral Oncol.* (2021) 116:105249. doi: 10.1016/j.oraloncology.2021.105249
- Chinn SB, Myers JN. Oral cavity carcinoma: current management, controversies, and future directions. *J Clin Oncol.* (2015) 33:3269–76. doi: 10.1200/JCO.2015.61.2929
- Dik EA, Willems SM, Ipenburg NA, Adriaansens SO, Rosenberg AJWP, Van Es RJJ. Resection of early oral squamous cell carcinoma with positive or close margins: relevance of adjuvant treatment in relation to local recurrence: margins of 3 mm as safe as 5 mm. *Oral Oncol.* (2014) 50:611–5. doi: 10.1016/j.oraloncology.2014.02.014
- Noorlag R, Klein Nulent TJW, Delwel VEJ, Pameijer FA, Willems SM, de Bree R, et al. Assessment of tumour depth in early tongue cancer: accuracy of MRI and intraoral ultrasound. *Oral Oncol.* (2020) 110:104895. doi: 10.1016/j.oraloncology.2020.104895
- Murakami R, Shiraishi S, Yoshida R, Sakata J, Yamana K, Hirose A, et al. Reliability of MRI-derived depth of invasion of oral tongue cancer. *Acad Radiol.* (2019) 26:e180–6. doi: 10.1016/j.acra.2018.08.021
- Tarabichi O, Kanumuri V, Juliano AF, Faquin WC, Cunnane ME, Varvares MA. Intraoperative ultrasound in oral tongue cancer resection: feasibility study and early outcomes. *Otolaryngol Head Neck Surg.* (2018) 158:645–8. doi: 10.1177/0194599817742856
- Idiyatullin D, Corum CA, Nixdorf DR, Garwood M. Intraoral approach for imaging teeth using the transverse B1 field components of an occlusally oriented loop coil. *Magn Reson Med.* (2014) 72:160–5. doi: 10.1002/mrm.24893
- Stens SCA, Bekers EM, Weijs WLJ, Litjens GJS, Veltien A, Maat A, et al. Evaluation of tongue squamous cell carcinoma resection margins using *ex-vivo* MR. *Int J Comput Assist Radiol Surg.* (2017) 12:821–8. doi: 10.1007/s11548-017-1524-6
- van der Kemp WJM, Klomp DWJ, Wijnen JP. 31 P T 2 s of phosphomonoesters, phosphodiester, inorganic phosphate in the human brain at 7 T. *Magn Reson Med.* (2018) 80:29–35. doi: 10.1002/mrm.27026
- Glunde K, Ackerstaff E, Natarajan K, Artemov D, Bhujwalla ZM. Real-time changes in 1H and 31P NMR spectra of malignant human mammary epithelial cells during treatment with the anti-inflammatory agent indomethacin. *Magn Reson Med.* (2002) 48:819–25. doi: 10.1002/mrm.10295
- Cao Z, Park J, Cho Z-H, Collins CM. Numerical evaluation of image homogeneity, signal-to-noise ratio, and specific absorption rate for human brain imaging at 1.5, 3, 7, 10.5, and 14T in an 8-channel transmit/receive array. *J Magn Reson Imaging.* (2015) 41:1432–9. doi: 10.1002/jmri.24689
- Schmitz AMT, Veldhuis WB, Menke-Pluijmers MBE, van der Kemp WJM, van der Velden TA, Kock MCJM, et al. Multiparametric MRI with dynamic contrast enhancement, diffusion-weighted imaging, and 31-phosphorus spectroscopy at 7 T for characterization of breast cancer. *Invest Radiol.* (2015) 50:766–71. doi: 10.1097/RLI.0000000000000183
- van der Kemp WJM, Stehouwer BL, Boer VO, Luijten PR, Klomp DWJ, Wijnen JP. Proton and phosphorus magnetic resonance spectroscopy of the healthy human breast at 7 T. *NMR Biomed.* (2017) 30:e3684. doi: 10.1002/nbm.3684
- Kappert KDR, Voskuilen L, Smeele LE, Balm AJM, Jasperse B, Nederveen AJ, et al. Personalized biomechanical tongue models based on diffusion-weighted MRI and validated using optical tracking of range of motion. *Biomech Model Mechanobiol.* (2021) 20:1101–13. doi: 10.1007/s10237-021-01435-7
- Löring J, van der Kemp WJM, Almujayyaz S, van Oorschot JWM, Luijten PR, Klomp DWJ. Whole-body radiofrequency coil for 31 P MRSI at 7 T. *NMR Biomed.* (2016) 29:709–20. doi: 10.1002/nbm.3517
- Rowland BC, Driver ID, Tachrount M, Klomp DWJ, Rivera D, Fornier R, et al. Whole brain 31P MRSI at 7T with a dual-tuned receive array. *Magn Reson Med.* (2020) 83:765–75. doi: 10.1002/mrm.27953
- van de Bank BL, Orzada S, Smits F, Lagemaat MW, Rodgers CT, Bitz AK, et al. Optimized 31P MRS in the human brain at 7 T with a dedicated RF coil setup. *Nmr Biomed.* (2015) 28:1570. doi: 10.1002/nbm.3422
- van Houtum Q, Welting D, Gosselink WJM, Klomp DWJ, Arteaga de Castro CS, van der Kemp WJM. Low SAR 31P (multi-echo) spectroscopic imaging using an integrated whole-body transmit coil at 7T. *NMR Biomed.* (2019) 32:e4178. doi: 10.1002/nbm.4178
- Raaijmakers AJE, Italiaander M, Voogt JJ, Luijten PR, Hoogduin JM, Klomp DWJ, et al. The fractionated dipole antenna: a new antenna for body

- imaging at 7 Tesla. *Magn Reson Med.* (2016) 75:1366–74. doi: 10.1002/mrm.25596
23. Meliàdo EF, Sbrizzi A, Berg CAT, Luijten PR, Raaijmakers AJE. Real-time assessment of potential peak local specific absorption rate value without phase monitoring: trigonometric maximization method for worst-case local specific absorption rate determination. *Magn Reson Med.* (2021) 85:3420–33. doi: 10.1002/mrm.28635
 24. Hoffmann J, Henning A, Giapitzakis IA, Scheffler K, Shajan G, Pohmann R, et al. Safety testing and operational procedures for self-developed radiofrequency coils. *NMR Biomed.* (2016) 29:1131–44. doi: 10.1002/nbm.3290
 25. Yarnykh VL. Actual flip-angle imaging in the pulsed steady state: a method for rapid three-dimensional mapping of the transmitted radiofrequency field. *Magn Reson Med.* (2007) 57:192–200. doi: 10.1002/mrm.21120
 26. Rodgers CT, Robson MD. Receive array magnetic resonance spectroscopy: whitened singular value decomposition (WSVD) gives optimal Bayesian solution. *Magn Reson Med.* (2010) 63:881–91. doi: 10.1002/mrm.22230
 27. Houtum Q, Mohamed Hoesein FAA, Verhoeff JJC, Rossum PSN, Lindert ASR, Velden TA, et al. Feasibility of ³¹P spectroscopic imaging at 7 T in lung carcinoma patients. *NMR Biomed.* (2019) 34:e4204. doi: 10.1002/nbm.4204
 28. NEN-EN-IEC 60601-1-2:2015 en. Available online at: https://www.nen.nl/nen-en-iec-60601-1-2-2015-en-211621?gclid=Cj0KCQjw sLWDBhCmARIsAPSL3_2qXJrUJXiFo1Pf2ADxkcIGEQA9OnmFPaqaPvYa9YmEm-k0tObAcaAss0EALw_wcB (cited April 7, 2021).
 29. Voskuilen L, de Heer P, van der Molen L, Balm AJM, van der Heijden F, Strijkers GJ, et al. A 12-channel flexible receiver coil for accelerated tongue imaging. *Magn Reson Mater Phys Biol Med.* (2020) 33:581–90. doi: 10.1007/s10334-019-00824-5
 30. Valković L, Dragonu I, Almujaayaz S, Batzakis A, Young LAJ, Purvis LAB, et al. Using a whole-body ³¹P birdcage transmit coil and 16-element receive array for human cardiac metabolic imaging at 7T. *PLoS One* . (2017) 12:e187153. doi: 10.1371/journal.pone.0187153
 31. Pohmann R, von Kienlin M. Accurate phosphorus metabolite images of the human heart by 3D acquisition-weighted CSI. *Magn Reson Med.* (2001) 45:817–26. doi: 10.1002/mrm.1110
 32. Birn RM, Bandettini PA, Cox RW, Jesmanowicz A, Shaker R. Magnetic field changes in the human brain due to swallowing or speaking. *Magn Reson Med.* (1998) 40:55–60. doi: 10.1002/mrm.1910400108
 33. Wijnen JB, Scheenen TWJ, Klomp DWJ, Heerschap A. ³¹P Magnetic resonance spectroscopic imaging with polarisation transfer of phosphomono- and diesters at 3T in the human brain: relation with age and spatial differences. *NMR Biomed.* (2010) 23:968–76. doi: 10.1002/nbm.1523
 34. Chang P, Nassirpour S, Henning A. Modeling real shim fields for very high degree (and order) B₀ shimming of the human brain at 9.4 T. *Magn Reson Med.* (2018) 79:529–40. doi: 10.1002/mrm.26658
 35. Marsman A, Lind A, Petersen ET, Andersen M, Boer VO. Prospective frequency and motion correction for edited ¹H magnetic resonance spectroscopy. *Neuroimage.* (2021) 233:117922. doi: 10.1016/j.neuroimage.2021.117922
 36. Boer VO, Klomp DWJ, Juchem C, Luijten PR, De Graaf RA. Multislice ¹H MRSI of the human brain at 7 T using dynamic B₀ and B₁ shimming. *Magn Reson Med.* (2012) 68:662–70. doi: 10.1002/mrm.23288
 37. Athar M, Raman R. Athar and Raman Case Report Correlating MRI and histological tumor thickness in the assessment of tongue cancer. *Asian Pacific J Heal Sci.* (2020) 7:22–7. doi: 10.21276/apjhs.2020.7.1.5

Conflict of Interest: RF was employed by company Ceresensa Inc.

The remaining authors declare that the research was conducted in the absence of any commercial or financial relationships that could be construed as a potential conflict of interest.

Publisher's Note: All claims expressed in this article are solely those of the authors and do not necessarily represent those of their affiliated organizations, or those of the publisher, the editors and the reviewers. Any product that may be evaluated in this article, or claim that may be made by its manufacturer, is not guaranteed or endorsed by the publisher.

Copyright © 2021 Forner, Nam, de Koning, van der Velden, van der Kemp, Raaijmakers and Klomp. This is an open-access article distributed under the terms of the Creative Commons Attribution License (CC BY). The use, distribution or reproduction in other forums is permitted, provided the original author(s) and the copyright owner(s) are credited and that the original publication in this journal is cited, in accordance with accepted academic practice. No use, distribution or reproduction is permitted which does not comply with these terms.